J. Quant. Spectrosc. Radiat. Transfer. Vol. 6, pp. 847–874. Pergamon Press Ltd., 1966. Printed in Great Britain

QUENCHING OF EXCITED ALKALI ATOMS AND RELATED EFFECTS IN FLAMES: PART II. MEASUREMENTS AND DISCUSSION

H. P. HOOYMAYERS and C. TH. J. ALKEMADE

Physical Laboratory, University of Utrecht, Netherlands

(*Received* 1 *March* 1966)

Abstract—An alternating current photoelectric device has been used for determining the yield factor p of resonance fluorescence of the yellow sodium doublet and the infrared and blue potassium doublets in flames at atmospheric pressure as a function of the temperature and composition of the burnt flame gases. From these measurements, the specific effective quenching cross section S (averaged over a Maxwellian velocity distribution) of the doublets considered for nitrogen, carbon dioxide, carbon monoxide, oxygen, hydrogen, argon, and water molecules could be derived. Remarkably, the S values for water molecules appeared to be very small compared to the values for the other diatomic and triatomic molecules. For nitrogen, carbon dioxide, hydrogen, and oxygen molecules, the specific effective quenching cross section appeared to be inversely proportional to the temperature in the range from 1700° to 2500°K. The S values found for the diatomic molecules H_2, N_2, and O_2 show a pronounced dependence on the resonance defect ΔE (that is, the difference between the alkali excitation energy and the nearest molecular vibrational energy). Large S values are associated with small energy defects. For a given ΔE value, however, the unsaturated diatomic carbon monoxide molecule shows a relatively large effective cross section, compared to the other diatomic molecules mentioned. Comparison of our S values with those reported in the literature yields further information about the dependence of S on the mean relative velocity of approach for sodium atoms in collision with nitrogen molecules. The effect of radiative nonequilibrium on the intensity of the outgoing flame radiation, as calculated in Part I of this paper for a spectral line with Lorentz broadening, was investigated by means of line-reversal temperature measurements as a function of atomic density in the flame. Also, the effect of radiative nonequilibrium on the shape of the emission curve of growth, as predicted in Part I for flames with a high yield factor p, was studied in experiments with a hydrogen–oxygen–argon flame.

1. INTRODUCTION

FOR A survey of the literature and of the major problems involved in the study of (de-) excitation mechanisms, we refer the reader to the introduction of Part I of this paper.[1]

2. THE EXPERIMENTAL SET-UP

The resonance fluorescence yield factor p, that is, the probability that an excited metal atom emits a photon before giving up its energy in a collision of the second kind (see Part I of this paper[1] was measured with the experimental set-up shown schematically in Fig. 1 (compare the work of BOERS *et al.*,[2] ALKEMADE,[3] and HOOYMAYERS[4]). A flame coloured with metal vapour was irradiated with a periodically interrupted light beam (50 c/s) from a Philips sodium or potassium lamp. The metal atoms in the flame partly absorbed this light and the intensity of the resonance fluorescence radiation emitted in a direction perpendicular to the incident light beam was measured with a vacuum phototube and an alternating current meter tuned at 50 c/s. The unmodulated radiation of the coloured flame was eliminated in this way.[5] Only the noise components at 50 c/s may

contribute to the meter fluctuations. A Beckman photopen recorder recorded the light pointer deflection of the tuned alternating current galvanometer[5] as a function of time in order to obtain greater accuracy by averaging the fluctuating signal.

An interference filter for selecting the desired radiation was placed at the entrance of the phototube to render the fluctuations caused by the flame background negligible with respect to the noise caused by the coloured flame. In addition, a diaphragm was

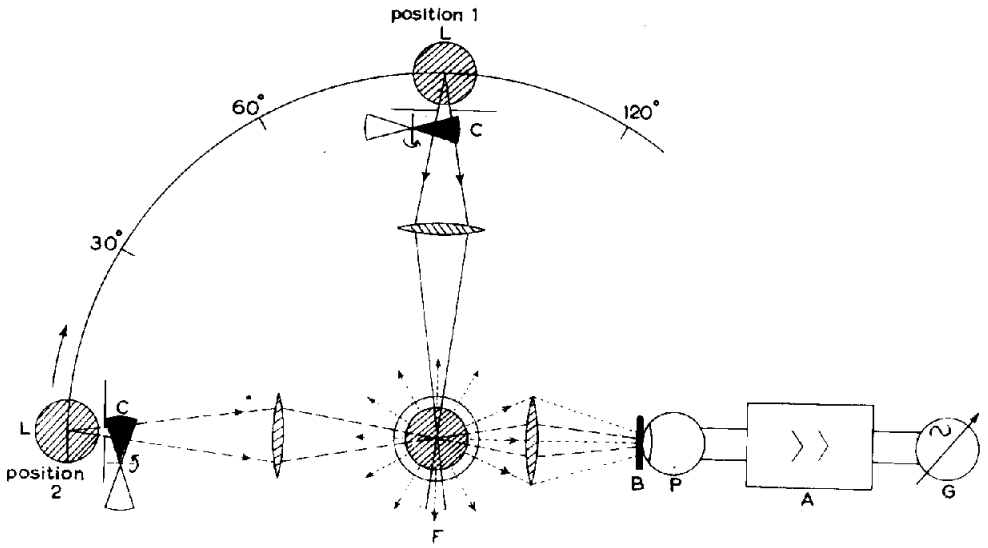

FIG. 1. Experimental arrangement for measuring the yield factor of resonance fluorescence: L = discharge lamp; C = periodic light chopper; F = shielded flame, coloured by metal vapour; B = filter; P = vacuum phototube; A = alternating current amplifier; and G = synchronous meter. The intensity of the fluorescence radiation is measured with L in Position 1, and the radiation flux absorbed in the flame is measured with L in Position 2.

placed between the flame and the phototube to ensure that light only from the part of the flame irradiated by the exciting lamp was received by the phototube. The flame gases, supplied from gas containers, first passed through pressure regulators which reduced the pressure to about 3 atm, and then they went through capillary valves which were used for precision regulation.[6]

The diluent gas, oxygen, and fuel were regulated separately and then were premixed before they entered the burner (see HOOYMAYERS[4]). The flowmeters were calibrated as described by HOLLANDER.[7] The Meker burner provided additional mixing of the gases and produced a stable, cylindrical, laminar flame. The gases had nominal purities between 99·5 per cent (carbon monoxide) and 99·9 per cent (argon), and they were used without further purification. The burner head consisted of concentric rows of exit channels having diameters ranging from 0·5 mm for oxygen–hydrogen–argon mixtures to 2·0 mm for oxygen–propane–argon mixtures.

The overall flames had an inner flame that was coloured by the presence of metal vapour, and this inner flame was shielded by a colourless burning mantle, which had the

same gas composition and temperature and moved with the same velocity as the inner flame. The flame mantle had the effect of providing a homogeneous temperature distribution in the coloured inner flame, and at the same time it prevented the infusion of nitrogen and oxygen from the surrounding air—a circumstance which would affect the p value in a sensitive way, especially in an argon flame.

The diameter of the inner flame at about 1 cm above the burner head was about 1·8 cm and the total flame diameter was 3·5 cm, so that the thickness of the flame mantle was about 1 cm. The total flame length—which ranged from 15 to 20 cm—as well as the total flame diameter, appeared to depend to some extent on the kind and composition of the entering gases, with the height of the cones varying between 0·2 and 0·5 cm for hydrogen–oxygen–argon and carbon monoxide–oxygen–nitrogen mixtures, respectively. To determine to what extent the inner flame was screened from the surrounding air by the mantle, we measured the fluorescence yield factor p for argon flames at varying heights.[4] From these experiments, it appears that practically no contamination occurred by mixing with air, up to a height of 3 cm above the burner head.

The metal salt solution was brought into the flame as a fine spray from an atomizer having a stainless steel needle for aspiration of the solution.[7] The performance of the sprayer appeared to deteriorate when high salt concentrations were used, this deterioration probably being caused by changes in the physical properties of the solution.[8] But all measurements could be corrected for this defect in spray performance, if necessary, by also reading the intensity of the band emission from calcium that had been added in uniform amounts to the alkali solution. Calcium was chosen because its band emission is not appreciably affected by self-absorption or by ionization at high salt concentrations; thus, the band intensity is proportional to the concentration of the calcium particles delivered by the sprayer to the flame.[4]

A survey of the flames that were used is shown in Table 1. The composition of the flame gases after combustion was calculated with an electronic computer by following the computer programme drawn up by ZEEGERS[9] and based on the general method outlined

TABLE 1. FLAME CHARACTERISTICS

Flame No.	Supplied gases (l/min)		Composition of burnt gases based on partial pressures (atm)				Temperature (°K)
1	H_2	1·72	H_2O	0·335	O_2	0·005	2350
	O_2	0·85	Ar	0·64	OH	0·006	
	Ar	3·45	H_2	0·01			
2	H_2	1·30	H_2O	0·29	O_2	0·003	2210
	O_2	0·65	Ar	0·70	OH	0·003	
	Ar	3·45	H_2	0·007			
3	H_2	1·00	Ar	0·75			2070
	O_2	0·50	H_2O	0·24			
	Ar	3·45	H_2	0·008			
4	H_2	1·72	H_2O	0·34	O_2	0·002	2160
	O_2	0·85	N_2	0·65	OH	0·002	
	N_2	3·45	H_2	0·006			
5	H_2	1·30	H_2O	0·29	O_2	0·001	1940
	O_2	0·65	N_2	0·70			
	N_2	3·45	H_2	0·002			

TABLE 1 (*Cont.*)

Flame No.	Supplied gases (l/min)		Composition of burnt gases based on partial pressures (atm)				Temperature (°K)
6	H_2	1·00	H_2O	0·245			1760
	O_2	0·50	N_2	0·75			
	N_2	3·45					
7	H_2	3·45	H_2O	0·31			1988
	O_2	0·92	N_2	0·58			
	N_2	2·03	H_2	0·10			
8	H_2	1·72	CO_2	0·55	H_2	0·002	2015
	O_2	0·86	H_2O	0·43	O_2	0·006	
	CO_2	2·30	CO	0·01			
9	H_2	1·30	CO_2	0·60	O_2	0·002	1790
	O_2	0·65	H_2O	0·395			
	CO_2	2·10	CO	0·003			
10	H_2	1·00	CO_2	0·66			1670
	O_2	0·50	H_2O	0·34			
	CO_2	2·10	CO	0·001			
11	H_2	1·72	H_2O	0·27			2095
	O_2	0·65	Ar	0·65			
	Ar	3·45	H_2	0·08			
12	H_2	1·72	H_2O	0·215			1850
	O_2	0·50	Ar	0·65			
	Ar	3·45	H_2	0·136			
13	H_2	1·00	H_2O	0·24			1990
	O_2	0·65	Ar	0·73			
	Ar	3·45	O_2	0·03			
14	H_2	1·00	H_2O	0·23	OH	0·001	1885
	O_2	0·86	Ar	0·70			
	Ar	3·45	O_2	0·072			
15	C_3H_8	0·30	CO_2	0·083	CO	0·022	2455
	O_2	1·50	H_2O	0·16	O_2	0·012	
	Ar	6·00	Ar	0·70	H_2	0·002	
			OH	0·008	H	0·007	
16	C_3H_8	0·30	CO_2	0·100	CO	0·008	2160
	O_2	1·50	H_2O	0·165	H_2	0·002	
	N_2	6·00	N_2	0·72	O_2	0·008	
17	CO	2·00	CO_2	0·275	CO	0·040	2385
	O_2	1·00	Ar	0·64	OH	0·003	
	Ar	4·00	H_2O	0·022	O_2	0·019	
18	CO	3·00	CO_2	0·145	H_2O	0·013	1700
	O_2	0·50	Ar	0·56	H_2	0·007	
	Ar	4·00	CO	0·275			
19	C_2H_2	0·50	CO_2	0·086	Ar	0·008	2600
	air	5·00	CO	0·106	N_2	0·69	
			H_2	0·014	O_2	0·003	
			H_2O	0·078			

by GAYDON and WOLFHARD.[10] Flame gas components contributing partial pressures smaller than 0·001 atm have not been entered in the table because their influence on the quenching of the excited alkali atoms is negligible in all cases.

The flame temperature was measured by the line-reversal method with the use of the accurate photoelectric device developed by SNELLEMAN.[6] At high metal concentrations,

the temperature could be determined to within an error of about 2°, whereas at low concentrations (that is, small optical thickness of the flame) the error was about 4°. By burning flames with constant hydrogen–oxygen ratio, but with varying ratios of diluent gas (argon, carbon dioxide, or nitrogen), we were able to produce stoichiometric hydrogen–oxygen flames with temperatures ranging from 1670° to 2350°K (see Table 1). These limits were set by flashback and blow-off of the flame.

3. THE MEASURING PROCEDURE

The yield factor p can be determined by the measured absorption of the light from the lamp in Position 2 (see Fig. 1) and the intensity of the fluorescent light (Position 1, Fig. 1), if we correct for the finite solid angle ω at which the fluorescent light is observed and for the ratio q of the sensitivities of the apparatus used in the two measurements, because of the difference in light intensity. We then have simply

$$p = \frac{u_r}{u_a} \cdot \frac{4\pi q}{\omega} \tag{1}$$

where u_r and u_a represent the meter deflections corresponding to the reemitted and absorbed radiation power, respectively. This equation is valid only when there is negligible self-absorption of the fluorescent radiation, that is, for low metal densities with the alkali first resonance lines.

At higher concentrations, corrections must be applied for the loss in fluorescent intensity due to self-absorption. Moreover, the absorption of the primary lamp radiation will not be uniform throughout the flame at high optical flame thickness, even when the concentration of metal atoms is constant in any flame cross section. To account for these effects, we have derived an expression, under simplifying conditions, for the intensity of resonance radiation that is emitted through a small solid angle ω in the direction perpendicular to both the incident light beam and the flame axis. The primary light is supposed to traverse the flame as a parallel, homogeneous beam having a small cross section, which intersects the flame axis at right angles. Furthermore, it is assumed that there is a uniform distribution of ground-state atoms N_0 throughout the cylindrical inner flame and that the peak absorption coefficient at the resonance frequency ν_0 is of the order of R^{-1}, at most. Here, R represents the radius of the circular flame cross section. Moreover, secondary resonance radiation, that is, re-emission of self-absorbed fluorescence light, was disregarded. Under these conditions, we found (see Fig. 2 and the Appendix to this paper) the following expressions for the radiation flux E_a absorbed from the exciting light beam and for the radiation flux E_r of the fluorescent light observed in a direction perpendicular to the exciting light beam:

$$E_a = \gamma_1 N_0 - \gamma_4 N_0^2 \tag{2}$$

and

$$E_r = p\frac{\omega}{4\pi}(\gamma_1 N_0 - \gamma_2 N_0^2) \tag{3}$$

where γ_1, γ_2, and γ_4 are positive constants and $p = A/(A+k_{-1})$ is the yield factor of resonance fluorescence. Here, A and k_{-1} represent the spontaneous radiative transition

probability per second and the probability per second for quenching collisions, respectively.

Combining equations (2) and (3) and using the expressions found for γ_1, γ_2, and γ_4 in the Appendix, we obtain

$$\frac{E_r}{E_a} = \frac{\omega}{4\pi} p \left[1 - N_0 \frac{(\gamma_2 - \gamma_4)}{\gamma_1}\right] = \frac{\omega}{4\pi} p \left(1 - N_0 \frac{\pi}{4} R \int_0^\infty \alpha_\nu \beta_\nu \, d\nu\right) \tag{4}$$

where $\alpha_\nu \, d\nu$ is the probability of an emitted photon having a frequency between ν and $\nu + d\nu$ and $\beta_\nu N_0 \, dx$ is the fraction of energy absorbed at frequency ν when the exciting light beam travels over a distance dx in the flame. Equation (4) shows a linear relationship

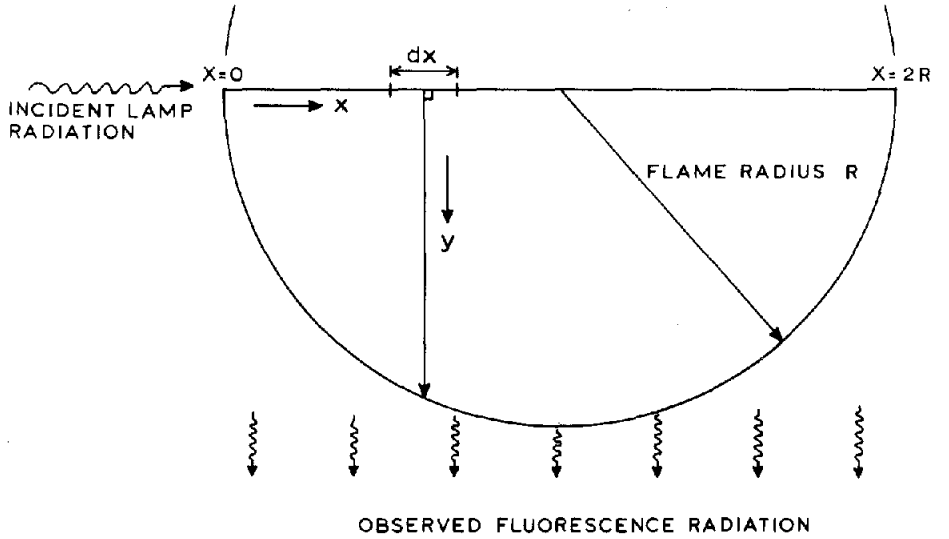

FIG. 2. Part of circular flame cross section, with co-ordinates as used in the text.

between E_r/E_a and N_0 for moderate metal densities, the slope of this relationship being proportional to p. In agreement with equation (1), it appears that E_r/E_a tends toward $(\omega/4\pi)p$ if N_0 goes to zero. According to this (asymptotic) linear relationship between E_r/E_a and N_0, accurate p values can be found by measuring $E_r/E_a (= qu_r/u_a)$ as a function of the metal solution concentration and then extrapolating to zero concentration. Moreover, this extrapolation allows us to neglect secondary and tertiary resonance radiation for all relevant p values ($p \lesssim 0{\cdot}4$).

4. DEPENDENCE OF FLAME ABSORPTION ON METAL CONCENTRATION

In Fig. 3, the absorbed primary radiation energy E_a (in per cent) is plotted as a function of the metal concentration in the sprayed solution. In agreement with equation (2), the double-logarithmic plot of absorption–density data for flame No. 2 (see Table 1) shows a slope of 45° for the yellow sodium doublet in the low density case and a decreasing

gradient for increasing metal concentration. It was found, however, that the absorption–density curve does not obey Beer's Law, this fact implying that the width of the exciting line and the width of the absorption coefficient of the flame, β_ν, are of comparable order. As expected, E_a tends toward 100 per cent when the concentration increases toward high

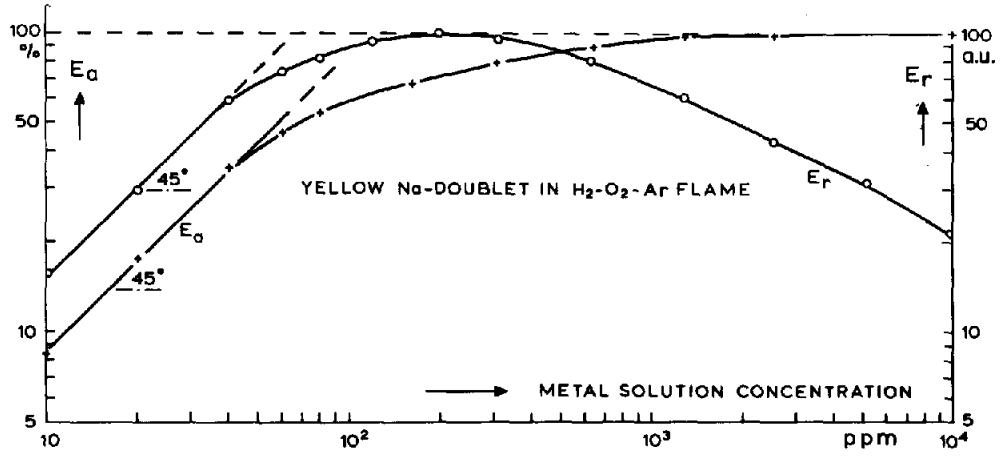

FIG. 3. Fraction E_a (per cent) of absorbed primary lamp radiation and reemission intensity E_r (arbitrary units) are plotted as functions of metal concentration in the sprayed solution for the sodium-D doublet in the hydrogen–oxygen–argon flame No. 2 (curves E_a and E_r, respectively).

values. This proves the absence of stray light, as well as of extraneous spectral lines emitted from the exciting lamp. Obviously, the width of the primary resonance line becomes less than the width of the flame absorption line in the high density case.

5. DEPENDENCE OF SODIUM FLUORESCENCE INTENSITY ON METAL CONCENTRATION

In agreement with equation (3), the double-logarithmic plot of the fluorescence intensity–density curve for flame No. 2 shows an initial slope of 45° for the yellow sodium doublet (see Fig. 3), followed by a decreasing gradient for increasing metal concentration. However, since at increasing metal densities the absorption of the primary light beam tends toward a maximum value (see discussion above) while the relative loss in fluorescence radiation due to self-absorption continues to increase to 100 per cent, the intensity of fluorescence radiation reaches a maximum value for a finite metal concentration, beyond which it decreases again to zero (see Fig. 3). The occurrence of an inversion in the "calibration curve" is well known, because of the analytical application of fluorescence flame photometry.[11]

In the derivation of equation (4), it is tacitly assumed that the intensity of the reemission radiation is isotropically distributed, so that the total reemission intensity can be obtained by multiplying the observed reemission intensity by $4\pi/\omega$. It was found experimentally that this assumption indeed holds true for metal concentrations up to 100 ppm. At higher

concentrations, the absorption of the incident light beam in the flame will not be uniform, and consequently, the intensity of the reemission radiation will not be uniformly distributed over the space directions.

6. DEPENDENCE OF THERMAL SODIUM EMISSION ON METAL CONCENTRATION (EMISSION CURVE OF GROWTH)

To check the predicted effect (see Part I[1]) of the underpopulation of the excited states, due to radiative non-equilibrium, on the shape of the emission curve of growth of the thermal flame emission, we measured the sodium flame emission in the absence of primary lamp radiation as a function of metal concentration (see Fig. 4). This was done by placing the modulating light chopper between the flame and the phototube (see Fig. 1).

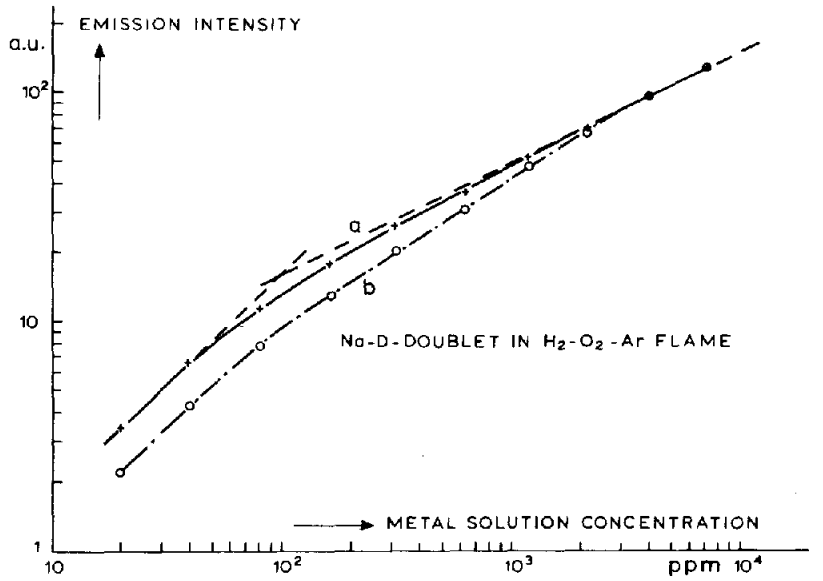

FIG. 4. Curves *a* and *b* show the emission curve of growth (intensity vs. metal concentration) for the sodium-*D* doublet in the hydrogen–oxygen–argon flame No. 2, after and before correction for radiative non-equilibrium, respectively. The initial and final slopes of the corrected curve correspond to tan = 1 and tan = ½, respectively, as expected theoretically. Both curves are corrected for any change in spray performance at high metal densities. Ionization effects were disregarded because of the low flame temperature.

Moreover, we were able to derive an absolute calibration of atomic metal concentration in the flame multiplied by the flame thickness, as well as of the so-called a' parameter[12] from the curve-of-growth measurements after correction for the effect of radiative non-equilibrium. The appropriate correction factor follows simply from the deviation of the line-reversal temperature from the true flame temperature, as described in Part I. The measurement of this deviation will be described in Section 10.

The absolute calibration of the metal flame content and knowledge of the a' parameter are essential in the quantitative interpretation of our experimental results concerning

the effects of radiative non-equilibrium (see discussion below). In the experimental derivation of the absolute metal content and a' parameter, we used the refined method of HOLLANDER[7] and VAN TRIGT,[13] who combined the emission curve of growth with measurements of the duplication factor (the latter is not affected by radiative non-equilibrium). All measurements of the curve of growth were corrected for deviations in the sprayer performance at high metal concentrations, as outlined in Section 2.

In Fig. 4, the dashed Curve b represents the measured curve of growth for the yellow sodium doublet in the hydrogen–oxygen–argon flame No. 2 (Table 1), corrected for deviations in spray performance. It should be noted that, because of the low flame temperature, depression of the atomic metal content in the flame by ionization can be disregarded. After correction for the effect of underpopulation in the excited state, it indeed appears that the initial and final asymptotes of the curve of growth have slopes corresponding to tan = 1 and tan = $\frac{1}{2}$, respectively, as would be expected for full thermal equilibrium (see solid Curve a in Fig. 4).

The plotted curves show that, especially for flames where the diluent gas consists for the most part of free atoms having a low quenching and excitation efficiency, the effect of radiative non-equilibrium leads to a noticeable downward parallel shift of the initial asymptote in the curve of growth. This results in an erroneously high value of the a' parameter when Hinnov's method is applied.[12]

In this method, the a' parameter is deduced from the intersection of the initial and final asymptotes of the curve of growth. One can easily conclude that the a' values found by HINNOV's method[7,12–15] are too high by a factor of $(1-p)$, owing to the radiative nonequilibrium effect. With the corrected curve of growth shown in Fig. 4, we found by following HOLLANDER's "combinatory method" that $a' = 1 \pm 0{\cdot}3$. The atomic metal content N_0 multiplied by the flame thickness $2R$ appeared to be equal to $(1{\cdot}9 \pm 0{\cdot}5) \times 10^{11}$ cm^{-2} for a sodium concentration of 100 ppm in the sprayed solution and for $2R = 1{\cdot}8$ cm. Under this condition, the relative absorption of the primary light beam amounts to 59 per cent.

7. MEASUREMENTS OF FLUORESCENCE YIELD FACTOR p

The ratio of the fluorescence intensity to the absorbed primary radiation power was measured as a function of the sprayed metal concentration. According to equation (4), a linear extrapolation of this ratio to zero concentration gives the true fluorescence yield factor p, free from self-absorption effects. The applicability of equation (4) is shown for a hydrogen–oxygen–argon flame (No. 2 in Table 1) in Fig. 5, where a linear dependence of this ratio on metal concentration appears to exist in the concentration range up to 80 ppm. It was found that the observed radiation was not caused by scattering in the flame. This fact was established by checking for the absence of any signal when the flame was illuminated by the yellow sodium radiation and when (a) no spray, (b) a spray of distilled water, and (c) a spray of potassium chloride solution, without sodium, were introduced into the flame. In all three cases, no absorption of sodium light was observed, either.

The slope of this linear relationship depends on the flame thickness and the sprayer performance, that is, on the ratio of metal concentration in the flame to the metal salt concentration in the sprayed solution. The same p value was found (after linear

extrapolation) with identical flames on which sprayers having different performance characteristics were used (see Fig. 5). It was found, too, that when use was made of identical sprayers on flames with different p values for a given spectral line, the slope of this linear relationship was proportional to the prevailing p value, in accordance with equation (4).[4] Here, a correction must be made for the differences in flame thickness.

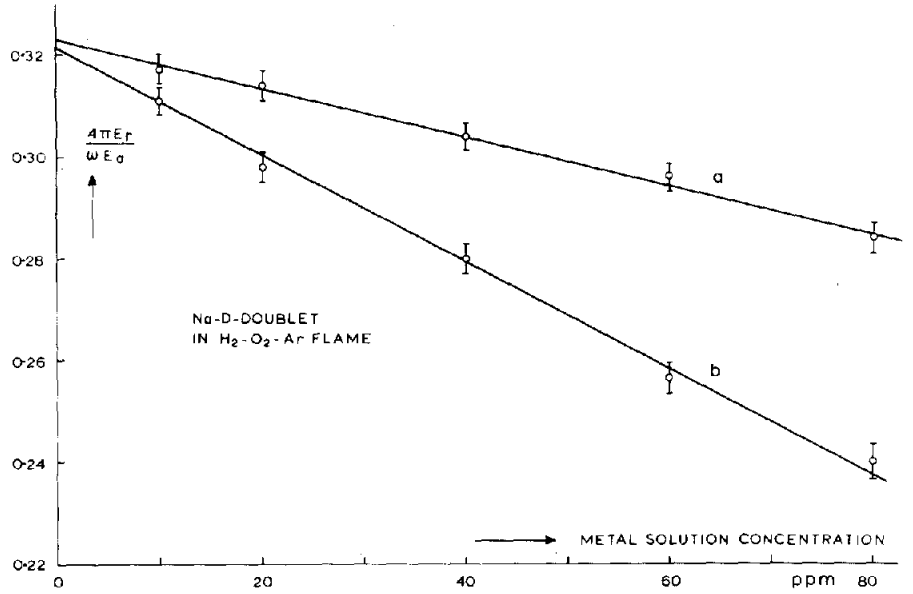

FIG. 5. Ratio of fluorescence intensity $(4\pi/\omega)E_r$ and absorbed primary radiation E_a as a function of metal solution concentration for the sodium-D doublet in the hydrogen–oxygen–argon flame No. 2. Curves a and b were obtained with identical flames, but with different sprayers. The p values (after linear extrapolation to zero concentration) appear to be equal to within 2 per cent for both curves.

This outcome implies that the absorption coefficient as a function of frequency does not change noticeably when the flame gas composition is changed. This conclusion agrees with the results obtained by HOLLANDER, who measured the a' parameter from the curve of growth for different flame gas compositions.[7,13]

Table 2 lists the experimental values of the yield factor p in different flames (see Table 1) for the yellow sodium doublet and the infrared and blue potassium doublets, and it also shows the number of quenching collisions during the natural lifetime, calculated from $k_{-1}/A = (1/p) - 1$. The listed p values are average values, obtained by repeating the measurements at least five times. The major source of error stems from the fluctuations of the thermal emission of the coloured flame at the measurement frequency, that is, at 50 c/s.[4]

For the yellow sodium doublet, the error in a single determination of the ratio of fluorescence intensity to absorbed radiation power in flames with small p values amounted to 3 to 6 per cent, depending on the solution concentrations. With the highest p value obtained, these errors amounted to 2 and 4 per cent, respectively. The magnitude of these errors still depends to some extent on the flame temperature, that is, on the intensity of the interfering thermal flame radiation. The final limits of error shown in Table 2 refer to the

results obtained after averaging and extrapolating the measurements that were made with different solution concentrations.

The most accurate results were obtained with the sodium doublet in the cool hydrogen–oxygen–argon flame having a high p value. The largest errors occur in measurements of the blue potassium doublet, for which the absolute magnitudes of the photoelectric

TABLE 2. MEASURED (AND CALCULATED) YIELD FACTORS FOR RESONANCE FLUORESCENCE

Excited state	$Na(3P_{1/2,3/2})$		$K(4P_{1/2,3/2})$		$K(5P_{1/2,3/2})$	
Wavelength (Å)	5890/96		7665/99		4044/47	
Optical transition probability $A(sec^{-1})$ (cf. Ref. 35)	$0{\cdot}63 \times 10^8$		$0{\cdot}37 \times 10^8$		$0{\cdot}019 \times 10^8$	
Relative error in p_{meas}	Flame no. 1, 2, 3, 11, 13 2% Flame no. 8, 9, 10, 18 4% Other flames 3%		Flame no. 2, 3, 11, 12 2% Flame no. 4, 6, 14 3% Flame no. 10, 18 4%		Flame no. 2, 3 10% Flame no. 12 15% Flame no. 6, 7 20%	
Flame no.	p_{meas}	K_{-1}/A	p_{meas}	K_{-1}/A	p_{meas}	K_{-1}/A
1	0·32 ($p_{calc} = 0{\cdot}32$)	2·1	—	—	—	—
2	0·32	2·1	0·40	1·5	$4{\cdot}0 \times 10^{-3}$	230
3	0·32	2·1	0·40	1·5	$4{\cdot}5 \times 10^{-3}$	230
4	0·039	25·	—	—	—	—
5	0·031	32·	0·044	21·5	—	—
6	0·026	38·	0·038	25·	8×10^{-4}	1200
7	—	—	—	—	9×10^{-4} ($p_{calc} = 7 \times 10^{-4}$)	—
8	0·019	52·	—	—	—	—
9	0·015	67·	—	—	—	—
10	0·012	81·	0·012	82·5	—	—
11	0·17	4·8	0·30	2·3	—	—
12	0·11	8·1	0·22	3·5	1×10^{-3}	1000
13	0·20	4·0	—	—	—	—
14	0·12	7·2	0·12	7·3	—	—
15	0·10 ($p_{calc} = 0{\cdot}099$)	9·2	—	—	—	—
16	0·026 ($p_{calc} = 0{\cdot}027$)	38·	—	—	—	—
17	0·042 ($p_{calc} = 0{\cdot}041$)	23·	—	—	—	—
18	0·021	47·	0·023	41·5	—	—
19	0·030 ($p_{calc} = 0{\cdot}031$)	31·	—	—	—	—

signals are very weak. This was due partly to the small power of the lamp emission and partly to the relatively small quantum efficiency of the phototube used at this wavelength. Moreover, the natural lifetime of the $5P$ state of potassium is comparatively long; thus, the effect of quenching collisions is large, resulting in a low p value.

It appeared that only with high potassium concentrations (that is, about 5000 ppm) could a reasonable signal–noise ratio be obtained for the blue potassium doublet. It was found experimentally that, even with such high metal densities, self-absorption of the blue potassium doublet can be disregarded, so that here, no extrapolation to low concentrations is required. For an oxygen-rich hydrogen–oxygen–argon flame, the absorption of lamp radiation in the case of the two potassium doublets appears to be four times

smaller than that in stoichiometric flames and hydrogen-rich flames, owing to the formation of potassium hydroxide in the flame and to the decrease in flame thickness. As a consequence, it was not possible to use oxygen-rich flames in determination of the fluorescence yield factor for potassium atoms in the $5P$ state, or to deduce from this the effective quenching cross section of oxygen molecules for this potassium doublet.

8. DERIVATION OF SPECIFIC EFFECTIVE QUENCHING CROSS SECTIONS AND THEIR TEMPERATURE DEPENDENCE

We have defined $S_{Na,j}$ as the specific effective quenching cross section of an excited sodium atom in the $3P$ state in collision with a flame particle of species j (see Part I[1]). In the derivation of $S_{Na,j}$ from the p values measured in flames of different composition and temperature (see equation (34) of Part I), we must make allowance for the unknown temperature dependence of each $S_{Na,j}$ separately. We solved this problem for oxygen, hydrogen, argon, and water molecules by a sort of iteration procedure by first deriving the approximate values of $S_{Na,Ar}$ and S_{Na,H_2O} by neglecting their temperature dependence, as well as neglecting the quenching effects of all other molecules present in the stoichiometric hydrogen–oxygen–argon flames (No. 1 and 2 in Table 1). It is seen in Table 1 that the burnt gases from these flames consist mainly of water and argon molecules.

TABLE 3. SPECIFIC QUENCHING CROSS SECTION S

Quenching species	Flame no.	T(°K)	$S\times10^{16}$ for $Na(3P_{1/2,3/2})$ (cm^2)	$S\times10^{16}$ for $K(4P_{1/2,3/2})$ (cm^2)	$S\times10^{16}$ for $K(5P_{1/2,3/2})$ (cm^2)
N_2	4	2160	36·±1·5	—	—
N_2	5	1940	40·±1·5	18·±0·6	—
N_2	6	1760	44·±1·5	19·±0·6	48·±10
CO_2	8	2015	94·±3	—	—
CO_2	9	1790	106·±3	—	—
CO_2	10	1670	113·±3	80·±2·5	—
H_2	11	2095	14·±0·5	3·4±0·1	—
H_2	12	1850	15·5±0·5	3·7±0·1	60·±10
O_2	13	1990	62·±2	—	—
O_2	14	1885	66·±2	31·5±1·0	—
CO	18	1700	85·±3	47·±1·5	—
Ar	2	2210	2·3±0·1	0·94±0·05	4·5±1
Ar	3	2070	2·3±0·1	0·94±0·05	4·5±1
H_2O	2	2210	1·0±0·06	0·42±0·02	5·±1
H_2O	3	2070	1·0±0·06	0·42±0·02	5·±1

Next, we computed S_{Na,H_2} and S_{Na,O_2} in a first approximation as a function of temperature (by using the S_{Na,H_2O} and $S_{Na,Ar}$ values that had just been found) from the measurements of p in fuel-rich and oxygen-rich hydrogen–oxygen–argon flames (No. 11 and 12 and No. 13 and 14, respectively, in Table 1). The first-order approximations of S_{Na,H_2} and S_{Na,O_2}, in turn, enabled us to derive more reliable values for the quenching cross section of argon and water molecules that were present in the burnt gases of flames No. 2 and 3. Repeating this procedure a few times led to the consistent set of values presented in Table 3.

Assuming that the relationship between $S_{Na,j}$ and T can be described as $S_{Na,j} \propto T^{-q/2}$ (see Part I), we can find q by plotting $S_{Na,j}(T)$ vs. T on double-logarithmic paper (see Fig. 6). From this plot, it follows that $q = 2 \pm 1$ for oxygen and hydrogen molecules.[4] Since the temperature dependence of S_{Na,H_2} and S_{Na,O_2} was investigated in a temperature range that extended over only about 100–250° (flames No. 11 through 14 in Table 1), the accuracy of the determination of q in this case was rather poor. It should be noted that our measurements do not allow us to determine the dependence of $S_{Na,Ar}$ and S_{Na,H_2O} on temperature. This holds true partly because of the small quenching effect of these particles and partly because the temperature range in our stoichiometric argon-cooled hydrogen flames was too small.

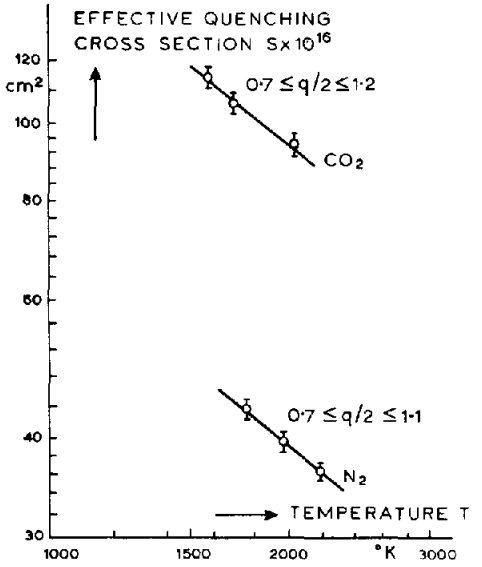

FIG. 6. The effective quenching cross section $S_{Na,j}$ for N_2 and CO_2 in collision with excited sodium (3P) atoms is shown as a function of flame temperature T. The term $q/2$ represents the slopes of these double logarithmic plots.

Our lack of knowledge about the temperature dependence of $S_{Na,Ar}$ and S_{Na,H_2O} hardly interferes with the computation of specific cross sections for the other molecules, because argon and water are ineffective quenchers. The effective quenching cross sections for sodium atoms in collision with nitrogen and carbon dioxide molecules, as well as their temperature dependences, were derived from the p values measured in flames No. 4, 5, and 6 and No. 8, 9, and 10, respectively, which cover a temperature range of 400°. In these flames, nitrogen and carbon dioxide, respectively, are supplied as "cooling gas" in major concentrations. So we can compute the values of S_{Na,N_2} and S_{Na,CO_2} and their temperature dependence by using the linear equations of the type of equation (34) of Part I, which can be written for each of the investigated flames. In these equations, the S values and the temperature dependence of S_{Na,H_2} and S_{Na,O_2} already found in the argon-cooled hydrogen–oxygen flames were inserted. We found also that, for nitrogen and carbon dioxide molecules, $q = 2 \pm 0{\cdot}4$ (see Fig. 6). Thus, we can conclude that the cross section $\sigma(v_r)$ varies roughly as v_r^{-2}, with the relative velocity v_r (see Part I) referring to H_2, O_2,

N_2, and CO_2 in collision with Na($3P$). Finally, the effective cross section $S_{Na,CO}$ was deduced from a carbon monoxide–oxygen–argon flame that was rich in fuel gas (No. 17 in Table 1).

Applying equation (34) of Part I and using the specific cross sections and their inverse T-dependence, we are now able to predict the p values for the more complicated flames, No. 1, 7, 15, 16, 17, and 19 (Table 1) and to compare them with the p values actually measured in these flames. The calculated and measured p values, p_{calc} and p_{meas}, are shown in Table 2 and are found to be in reasonable agreement with each other. This agreement confirms the assumed T-dependence of the cross sections that was considered, since flames No. 1, 7, 15, 16, 17, and 19 differ not only in gas composition, but also in temperature.

TABLE 4. COMPARISON OF RESONANCE DEFECT ΔE WITH MEASURED SPECIFIC EFFECTIVE QUENCHING CROSS SECTION S

Quenching species	Atomic excitation level and excitation energy (eV)		Vibrational quantum number v, and energy E of nearest molecular level (eV)		ΔE (eV)	$S \times 10^{16}$ at 2000°K (cm^2)
			v	E		
N_2	Na($3P_{1/2,3/2}$)	2·105	7	1·952	−0·152	39·
			8	2·215	+0·111	
CO	Na($3P_{1/2,3/2}$)	2·105	8	2·038	−0·066	72·
			9	2·279	+0·175	
H_2	Na($3P_{1/2,3/2}$)	2·105	4	1·888	−0·216	14·
			5	2·290	+0·186	
$O_2(^3\Sigma)$	Na($3P_{1/2,3/2}$)	2·105	11	1·969	−0·135	62·
			12	2·135	+0·032	
$O_2(^1\Delta)$	Na($3P_{1/2,3/2}$)	2·105	6	2·047	−0·057	62·
			7	2·213	+0·109	
$O_2(^1\Sigma)$	Na($3P_{1/2,3/2}$)	2·105	3	2·150	+0·046	62·
N_2	$K(4P_{1/2})$	1·613	5	1·411	−0·216	17·5
			6	1·682	+0·069	
	$K(4P_{3/2})$	1·620			−0·209	
					+0·062	
CO	$K(4P_{1/2})$	1·613	6	1·547	−0·066	40·
			7	1·794	+0·181	
	$K(4P_{3/2})$	1·620			−0·073	
					+0·174	
H_2	$K(4P_{1/2})$	1·613	3	1·461	−0·152	3·5
			4	1·888	+0·275	
	$K(4P_{3/2})$	1·620			−0·016	
					+0·268	
$O_2(^3\Sigma)$	$K(4P_{1/2})$	1·613	8	1·464	−0·149	30·
			9	1·634	+0·021	
	$K(4P_{3/2})$	1·620			−0·156	
					+0·014	
$O_2(^1\Delta)$	$K(4P_{1/2})$	1·613	3	1·524	−0·089	30·
			4	1·698	+0·085	
	$K(4P_{3/2})$	1·620			−0·096	
					+0·078	
$O_2(^1\Sigma)$	$K(4P_{1/2})$	1·613	0	1·638	+0·025	30·
	$K(4P_{3/2})$	1·620			+0·018	
N_2	$K(5P_{1/2,3/2})$	3·070	11	2·982	−0·088	46·
			12	3·242	+0·172	
H_2	$K(5P_{1/2,3/2})$	3·070	7	3·014	−0·055	58·
			8	3·415	+0·345	

9. RESONANCE EFFECTS IN THE QUENCHING PROCESS

For some diatomic molecules (CO, O_2, H_2, and N_2) and for all three of the atomic doublets mentioned, we investigated the correlation between the effective quenching cross section at 2000°K and the resonance defect ΔE (that is, the energy difference between the atomic excitation level and the nearest vibrational level of the quenching molecule). Table 4 shows the relevant energy values for the investigated quenching process, together with the specific quenching cross sections, either found at 2000°K or converted thereto.

The molecular vibrational energy values were calculated from data in the literature.[16] In this calculation, only the transitions from molecular vibrational ground states were taken into account, although, for the sodium-*D* doublet for example, the ΔE values will be less by 0·03 eV at most, when the $v = 1$ vibrational levels of O_2, N_2, and H_2 are considered. Using the relationship between S and ΔE shown in Fig. 6 as a first approximation, one expects an increase in S value amounting to 17, 26, and 50 per cent, respectively, for the $v = 1$ levels of O_2, N_2, and H_2. Since the populations of the $v = 1$ levels are less by factors of three, five, and nine, respectively, than those at the $v = 0$ levels for these molecules at $T = 2000$°K, the error introduced in the establishment of the $S-\Delta E$ relationship by disregarding the $v \geq 1$ levels is not serious for the sodium-*D* doublet. For carbon monoxide molecules, this neglect is the more justified, because ΔE *increases* when the $v = 1$, instead of the $v = 0$, level is considered. Because of similar considerations, we can also disregard the transitions from the vibrational states with $v \geq 1$ for the other alkali lines mentioned.

In the case of molecular oxygen as a quencher, we must allow for the occurrence of three different electronic states having excitation energies smaller than the excitation energy of the alkali atoms. We have assumed that in the quenching collision with O_2 the alkali excitation energy can be converted into combined electronic and vibrational excitation energy, because transfer of energy to the $^1\Delta$ and $^1\Sigma$ electronic states of O_2 is not restricted by Wigner's spin conservation rule. In the comparison of the effective cross sections for this molecule with those for the other diatomic molecules on the basis of their resonance defects, we thus must allow for the statistical weight factors of the mentioned electronic O_2 levels, each yielding a different resonance defect ΔE (see Table 4). Fortunately, the $^3\Sigma$ level of O_2 having the smallest resonance defect with respect to the excited Na(3*P*) state also has the largest statistical weight factor. So we can treat O_2 as a quencher on the basis of a value $\Delta E = 0{\cdot}031$ eV for the yellow sodium doublet, which holds for the $^3\Sigma$ levels, and disregard the other two electronic levels. Through similar considerations, we can treat O_2 as a quencher of the infrared potassium doublet by assuming a resonance defect $\Delta E = 0{\cdot}014$, which, strictly speaking, holds only for the $^3\Sigma$ state of O_2.

In Fig. 7, S is plotted as a function of $|\Delta E|$ for the diatomic molecules investigated. As long as $|\Delta E|$ is much less than kT, we can assume that the quenching cross section is a symmetrical function of ΔE. This means that it does not make any difference whether a small amount of translational or rotational energy is consumed or produced in the quenching process. In the derivation of the quenching cross section S, an activation factor (the Boltzmann factor) should be taken out for those molecules that have a vibrational level that is closest to, and of energy that is higher than, the electronic energy of the alkali metal concerned (endothermic quenching); see Table 4.

The worst case occurs for hydrogen as a quencher of excited Na($3P$), having a vibrational level exceeding the sodium excitation level by 1·04kT. If we allow for the activation factor, the "true" quenching cross section might exceed the plotted S value by 35 per cent. The actual error in the plotted S value will be less, because a part of the quenching of excited sodium atoms also occurs probably through the H_2 level lying

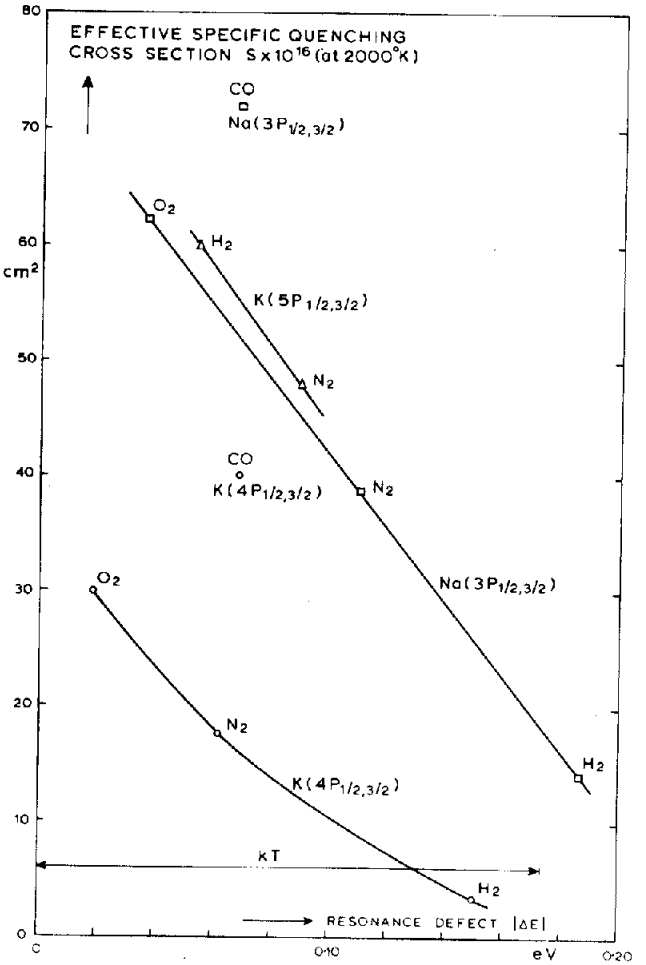

FIG. 7. The effective specific quenching cross sections S (at 2000°K) for some diatomic molecules (CO, O_2, H_2, and N_2) in collision with excited sodium atoms in the $3P_{1/2,3/2}$ state and excited potassium atoms in the $4P_{1/2,3/2}$ and $5P_{1/2,3/2}$ states are plotted as functions of the resonance defect. The value of kT at 2000°K is indicated by an arrow drawn parallel to the abscissa.

0·216 eV below (exothermic quenching) the Na excitation energy (see Table 4), which requires no activation factor. Incidentally, the value $|\Delta E|$ is almost the same for the two H_2 levels discussed. Moreover, the deficit in energy in the endothermic quenching process by H_2 may be supplied from more than one degree of freedom (for example, from relative motion or rotation), so that the above estimate of 35 per cent will be too high. In the other cases of endothermic quenching processes in Fig. 7 (see Table 4), the influence of

the activation factor will be less than 20 per cent and 3 per cent for quenching of Na(3*P*) by N_2 and O_2, respectively, and less than 10 per cent and 2 per cent for quenching of K(3*P*) by N_2 and O_2, respectively.

It is of no use to correct for the errors due to activation factors, since the difference in kinetic cross section of the quenching particles is not accounted for in the plot of the resonance curve. This difference introduces an uncertainty in the true resonance curve, which is of the same order—for example, in the case of H_2 and O_2 (or N_2) molecules in collision with sodium atoms, the difference in kinetic cross section amounts to about 15 per cent. Figure 7 shows that a small energy defect is associated with a relatively large quenching cross section. Furthermore, it appears that the quenching cross section for K(5*P*) atoms in collision with diatomic molecules is systematically larger than for K(4*P*) atoms. This outcome is not surprising. The *S* values for the carbon monoxide molecules do not appear to fit the curve through the points obtained with the other diatomic molecules (we shall discuss this outcome below).

We have also calculated energy differences between the 3*P* level of Na and some neighbouring vibrational levels of the water molecule derived from the literature.[17] Resonance defects were found to be smallest with the (4, 0, 1) and (3, 0, 2) vibrational levels combining with the ground state level, and to amount to 0·066 and 0·076 eV, respectively. Obviously, the small quenching cross section of H_2O in collision with excited sodium atoms cannot be explained on the basis of a resonance defect, which is even smaller for H_2O than for the diatomic molecules. The anomalously small cross section of H_2O contrasts with the quenching effect of the other triatomic molecule that was investigated, CO_2.

10. MEASUREMENTS OF LINE-REVERSAL TEMPERATURE AS A FUNCTION OF METAL CONCENTRATION

In Part I,[1] expressions were derived for the deviation ΔT of the line-reversal temperature T_e from the true flame temperature T_t as a result of radiative non-equilibrium; this was done for both the low and high density cases (see equations 26 and 29 of Part I). In these expressions, which depend on the spectral line profile, the resonance fluorescence yield factor p appears as a parameter. Large deviations are to be expected in the cases of high p values and low metal densities. In the case of a Lorentzian line profile, and with high metal densities, it follows from equation (25) of Part I that

$$\Delta T = \text{constant}./N_0^{-1/2} \tag{5}$$

where N_0 is the ground state atom concentration in the flame. This behaviour is also expected to hold true for mixed Lorentz and Doppler broadening of the metal spectral line. The proportionality constant may then have a different value, which has not been calculated here. In order to check the validity of equation (5) and of equation (29) in Part I, we measured the increase in line-reversal temperature as a function of the sodium concentration in the sprayed solution, which is proportional to N_0 after correction is made for possible alterations in the sprayer performance at high salt concentrations (see Section 1 and Fig. 8).

A hydrogen–oxygen–argon flame was chosen because large p values occur with that mixture. Because of equation (5) we have, in the high density limit for a Lorentzian (or

mixed) line profile,

$$\frac{T_e(c_2)-T_e(c_1)}{T_e(c_3)-T_e(c_2)}=\frac{(c_2/c_1)^{1/2}-1}{1-(c_2/c_3)^{1/2}} \tag{6}$$

where c_1, c_2, and c_3 represent three different metal concentrations in the solutions. In this equation, the unknown constant of proportionality from equation (5) and the as yet unknown true flame temperature drop out. If c_3 tends toward infinity, then $T_e(c_3)$ approaches T_t, so that we have

$$T_t=\frac{T_e(c_2)-T_e(c_1)}{(c_2/c_1)^{1/2}-1}+T_e(c_2). \tag{7}$$

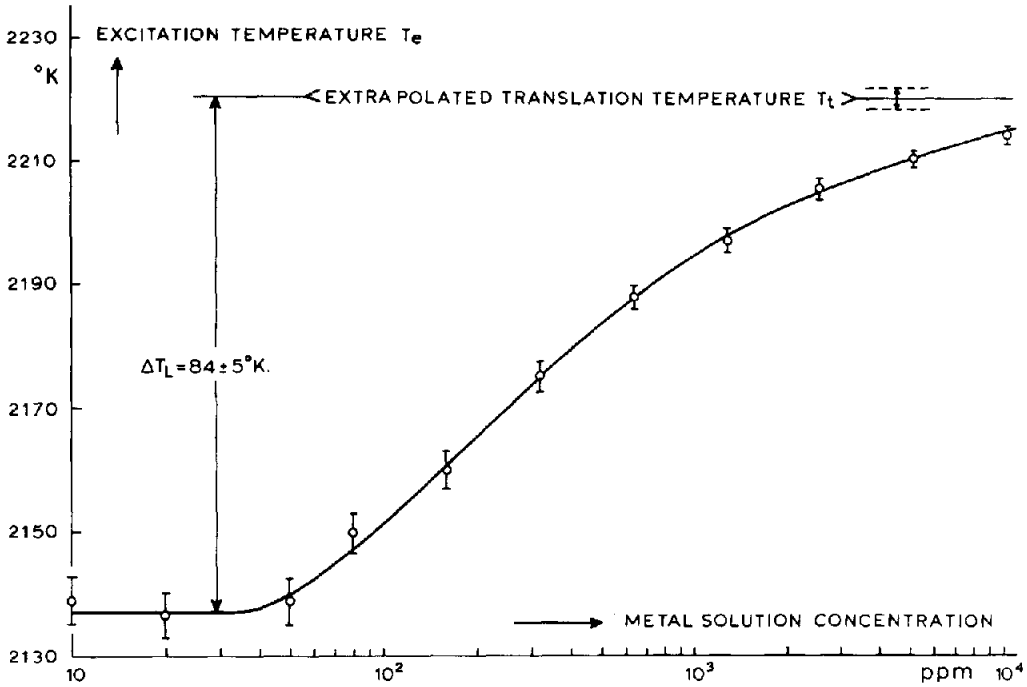

FIG. 8. Excitation temperature T_e, measured by sodium line reversal, is plotted as a function of the sodium solution concentration for the shielded hydrogen–oxygen–argon flame No. 2. The symbol ΔT_L represents the deviation of T_e from the true (translation) temperature T_t in the limiting case of low metal concentration, as found by extrapolation from the high-density values of T_e (cf. text).

These expressions enable us to check equation (5) and to find T_t when we spray solutions having sufficiently high metal concentrations. Once T_t is known, we find from Fig. 8 that, for the deviation ΔT_L in line-reversal temperature for *low* metal densities,

$$\Delta T_L = 84\pm4°\text{K}.$$

Inserting $p = 0{\cdot}32$ (see Table 1 for flame No. 2) in equation (26) of Part I, we calculate

$$\Delta T_L = 80\pm3°\text{K}$$

in agreement with the above experimental result.

Conversely, the fluorescence yield factor p could also be found with satisfactory accuracy from the rise in the excitation temperature with increasing metal concentration, provided that p is not too small and that accurate measurements of line-reversal temperatures are possible.

Upon plotting the deviation of the excitation temperature from the true flame temperature as a function of c (with c being the solution concentration) on double logarithmic paper, we obtain a straight line with a slope corresponding to $\tan = \frac{1}{2}$ if c exceeds 200 ppm (see Fig. 9). This outcome confirms the validity of equation (5) for the yellow sodium doublet in the high density case for the hydrogen–oxygen–argon flame under consideration.

The knowledge of the absolute metal flame content N_0 and the a' parameter for the hydrogen–oxygen–argon flame (see Section 6) enables us to make a more nearly quantitative check of our calculations in Part I, concerning the effect of radiative non-equilibrium. In particular, we are then able to calculate the constant of proportionality in equation (5) for pure Lorentz broadening and to compare this with the experimental value (see Part I). Equation (29) of Part I relates ΔT to the fractional defect in the emitted radiation intensity, $\alpha(\xi_c)$, whereas equation (25) of Part I in its turn relates $\alpha(\xi_c)$ to the dimensionless flame thickness $\xi_c = \kappa_m L$, which involves N_0 and a'.

If the line profile is determined by a combined Lorentz damping and Doppler broadening, we have, according to classical theory[18]

$$\kappa_m = \kappa_0 \frac{a'}{\pi} \int_0^\infty \frac{\exp(-y^2)}{y^2 + a'^2}\, dy \tag{8}$$

where

$$\kappa_0 = 2\pi^{1/2} \frac{e^2}{m_e c} \frac{N_0 f (\ln 2)^{1/2}}{\Delta \nu_D} \tag{9}$$

and *

$$a' = \frac{\Delta \nu_L}{\Delta \nu_D} (\ln 2)^{1/2} \tag{10}$$

where $\Delta \nu_D$ and $\Delta \nu_L$ represent the Doppler and Lorentz widths, respectively, at half-maximum of the absorption coefficient. The other quantities have their usual meaning.[12] The value of κ_m is listed for several values of a' by MITCHELL and ZEMANSKY,[18] and it appears to be equal to $0{\cdot}42\kappa_0$ for $a' = 1$. Using equation (9), with

$$\Delta \nu_D = (\nu_0/c)(8kT_i/m)^{1/2}(\ln 2)^{1/2},$$

and inserting $L = R$ (= flame radius), we find that $\xi_c = \kappa_m R = 10$ for $N_0 R = 5{\cdot}7 \times 10^{12}\,\mathrm{cm}^{-2}$. This value of $N_0 R$ corresponds to a sodium concentration in the sprayed solution of 6000 ppm.

By inserting this value of ξ_c in equation (24) of Part I for $\alpha(\xi_c)$, which has been derived for a pure Lorentz broadened resonance line in the high density case, we find by graphical integration that $\alpha(10) = 0{\cdot}035$. Through equation (29) of Part I, this finally yields

* Owing to the rather large p value ($p \simeq \frac{1}{3}$) measured in the hydrogen–oxygen–argon flame, we can neglect the term $(1/p)(A/2\pi)$, which makes allowance for the broadening effect of quenching collision, in comparison to $\Delta \nu_L$ (see equation (31) of Part I).

$\Delta T_{calc}^{Lor} = 7°K$ for the calculated deviation of excitation temperature in the case of pure Lorentz broadening and $(N_0)^{1/2}\Delta T_{calc}^{Lor} = 1{\cdot}8 \times 10^7\ cm^{-3/2}°K$ for the constant of proportionality in equation (5).

This value appears to deviate 25 per cent from the measured value of the proportionality constant, corresponding to the measured temperature deviation, $\Delta T_m = 9{\cdot}5°K$

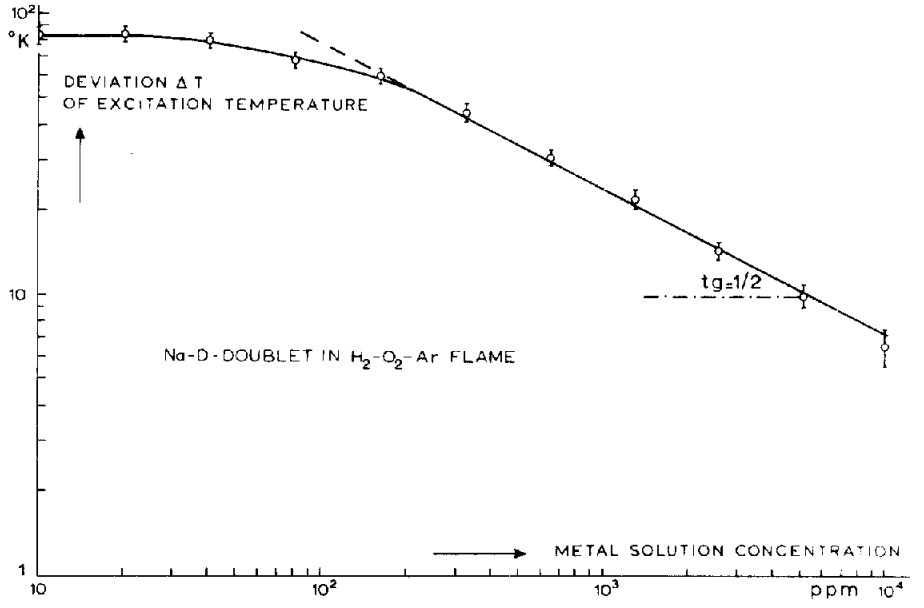

FIG. 9. Double logarithmic plot of the deviation ΔT of excitation temperature T_e from true flame temperature T_t as a function of metal solution concentration (as derived from Fig. 8). Note that, with high solution concentration, ΔT varies as $1/(N_0)^{1/2}$, as predicted by theory for a Lorentzian line shape.

(see Fig. 8). Apparently, the formula derived for a pure Lorentz line profile in the high density case can also be applied as a reasonably good approximation for mixed Doppler and Lorentz line profiles. This holds true at least for $a' \geq 1$. For a pure Doppler line shape we have, because of similar calculations, that $\Delta T_{calc}^{Dop} = 20°K$ for the same sodium concentration in the flame, so that $\Delta T_{calc}^{Lor} < \Delta T_m < \Delta T_{calc}^{Dop}$ is valid, a circumstance which can be expected *a priori* for actual flames with mixed Doppler and Lorentz line profile.

II. CONSIDERATION OF NONUNIFORM METAL DENSITY

In the derivation of the expression for ΔT in the high density case, a uniform density of ground state atoms was assumed to exist throughout the coloured inner flame. However, outward diffusion from the inner flame to the colourless flame mantle may cause a gradual decrease of metal concentration toward the flame border.

In Part I,[1] an expression has been derived for the characteristic thickness of the layer in which the major drop in density occurs. If we assume the value $D = 8\ cm^2/sec$, as found by SNELLEMAN,[6] for the diffusion coefficient of Na, $v = 600\ cm/sec$ for the rise

velocity of the flame gases, and $z = 0{\cdot}5$ cm for the height of measurement above the burner head, then equation (30) of Part I will yield a value of 0·3 cm for the characteristic thickness of the diffusion layer. For a solution concentration of 10 000 ppm of sodium, this thickness is of the order of $2\kappa_m^{-1}$. Nevertheless, quantitative agreement was found to exist between our measured and calculated ΔT values (see discussion above), while the measured values of ΔT appeared to vary with metal concentration in the high density case up to the highest concentrations investigated, as predicted by theory [equation (5)]. So we can conclude that diffusion effects are negligible up to the concentrations for which $\kappa_m^{-1} = 0{\cdot}15$ cm.

This outcome is perhaps not so surprising (with regard to the fairly large thickness of the diffusion layer) if one remembers that, with pure Lorentz line profiles and combined Lorentz and Doppler line shapes, a noticeable part of the outgoing radiation is emitted in the spectral line wings. At these frequencies the absorption coefficient is markedly less than κ_m, and the emitted radiation stems from flame depths exceeding the diffusion layer thickness.

12. CONSIDERATION OF NON-UNIFORM TEMPERATURE DISTRIBUTION

In our calculations, a uniform temperature throughout the flame was assumed. The absence of radial T variations in our coloured flame section, which was shielded by a colourless flame mantle of similar composition (see Section 2), can be concluded from the observation that the excitation temperature is independent of sodium concentration within the error limits (about 5°K) in the carbon dioxide cooled hydrogen–oxygen flame No. 8 (see Table 1 and HOOYMAYERS[4]).

It should be noted that the very low p value of this flame (see Table 2) ensures that the reversal temperature will be virtually equal to the true flame temperature at any sodium concentration. If there should be a radial drop in temperature in the coloured flame, however, then self-reversal would occur and the measured reversal temperature would systematically decrease with increasing sodium concentration. So the invariance of the measured reversal temperature with the sodium concentration in this flame points to a uniform radial temperature distribution. This result supports the consistency found among the results obtained with different metal concentrations in the more general case of an arbitrary p value. Any radial variation of true flame temperature would show up more markedly with the higher metal concentrations, at which the optical flame thickness is correspondingly larger. Moreover, it was experimentally found that no relevant variation in flame temperature occurs in the cases of sodium concentrations in the sprayed solution that were more than 2000 ppm, over a height interval of the order of $2\kappa_m^{-1}$. So our results were not affected by a non-uniform temperature distribution in the vertical direction, either.

13. CONSIDERATION OF THE FREQUENCY-DEPENDENT POPULATION FUNCTION

Finally, it should be noted that in our calculation of $\alpha(\xi_c)$ we essentially used the assumption that the frequency at which a photon is absorbed and the frequency at which it may be re-emitted are completely uncorrelated (see Part I[1]). One may expect that this

condition is fulfilled when an excited sodium atom suffers many "perturbing adiabatic collisions" during its actual radiative lifetime. This radiative lifetime is affected by quenching collisions and it can be put equal to p/A (see Part I).

By using the experimental value of $\Delta\nu_L$ found for the hydrogen–oxygen–argon flame under consideration, we obtain for the average number of perturbing adiabatic collisions per actual radiative lifetime, $(p/A)R_L \approx 120$. Here, $R_L = \pi\Delta\nu_L$ represents the collision frequency of Lorentz collisions. From this outcome and from Hearn's considerations[19] on the effect of a frequency-dependent population function in the case of Doppler broadened spectral lines, we learn that for the hydrogen–oxygen–argon flame under consideration a frequency-independent population function can safely be used.

14. COMPARISON WITH THE LITERATURE DATA AND FINAL CONCLUSIONS.

Quenching cross sections for collisions in which internal energy is exchanged between an excited sodium atom and a quenching flame particle have already been reported in the literature for various kinds of quenching species under different measurement conditions. Comparison of our values with other experimental results may yield additional information on the dependence of S on the mean relative velocity of approach of the particles involved in the quenching collision.

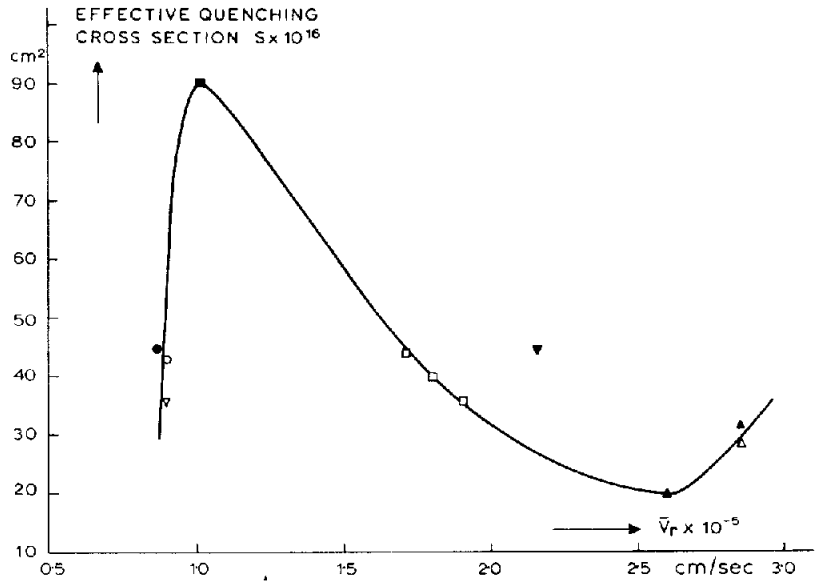

FIG. 10. Effective quenching cross section S of excited sodium ($3P$) atoms in collision with nitrogen molecules for various (mean) relative velocities $\bar{v}_r$ of the colliding species, as inferred from the literature and from this work (cf. Table 5).

● NORRISH and SMITH
○ DEMTRÖDER
□ This work
▲ KISELBASCH, KONDRATIEV and LEIPUNSKII
▽ HULPKE, PAUL and PAUL
■ VON HAMOS
▼ TSUCHIYA
△ WINANS

MITCHELL and ZEMANSKY[18] have reported measurements, which have been performed by TERENIN and PRILESHAIEVA,[20] by WINANS,[21] and others, on the quenching of excited sodium ($3P$) atoms by various kinds of quenching molecules. In these experiments, the excited sodium atoms are produced by optical dissociation of sodium iodide vapour by photons having wavelengths of 2430 Å or less to form an excited sodium atom and a normal iodine atom. When the dissociation is accomplished by means of light from metal sparks having wavelengths shorter than 2430 Å, the excess energy is transformed into relative translational energy of the atoms produced.

By varying the wavelength of the exciting radiation, the velocity of the excited sodium atoms can be varied at will. MITCHELL and ZEMANSKY have calculated, for the different wavelengths applied, the velocity v_{Na} with which the excited sodium atom escapes from the sodium iodide molecule upon dissociation. This velocity of escape is uniformly distributed with regard to directions in space, as was shown by MITCHELL.

For sufficiently short wavelengths, the quenching particles can be regarded as being stationary in comparison to the velocity of the excited sodium atoms, so that we can write $\bar{v}_r = v_{Na}$ for the mean relative velocity of approach $\bar{v}_r$ of the colliding particles. However, for a small excess of energy in the dissociating light quantum or for fast moving quenching particles having a Maxwellian velocity distribution (as occurs with high temperatures or with hydrogen molecules), the v_r occurring in equation (34) of Part I should better be calculated from $\bar{v}_r = (\bar{v}_{Na}^2 + \bar{v}_j^2)^{1/2}$. Here, $\bar{v}_j$ is the mean velocity of the quenching particle. When necessary, we have replaced the v_{Na} values used by MITCHELL and ZEMANSKY in the calculation of cross sections by the mean values $\bar{v}_r$. In Fig. 10, we have plotted the effective quenching cross sections of excited sodium ($3P$) atoms in collision with nitrogen molecules for various relative velocities, v_r or $\bar{v}_r$, of the colliding species, as derived from the work of WINANS,[21] VON HAMOS,[22] KISELBASCH, *et al.*,[23] HULPKE, *et al.*,[24] DEMTRÖDER,[25] TSUCHIYA,[26] and NORRISH and SMITH,[27] and from our own work (see also Table 5). When the velocities of both kinds of colliding particles show a Maxwell distribution (as in our experiments), we calculated the cross section from the collision frequency by inserting $\bar{v}_r = (\bar{v}_{Na}^2 + \bar{v}_{N_2}^2)^{1/2}$ in equation (34) of Part I.

In agreement with the experiments on the quenching of excited sodium ($3P$) atoms by iodine and bromine molecules,[12] we learn from Fig. 10 that S decreases with increasing $\bar{v}_r$ for relatively large v_r values.

In Part I[1] of this paper, we showed that the exponent q in the relation,

$$\sigma(v_r) = (\text{constant}) v_r^{-q} \tag{11}$$

can be derived from the dependence of the *effective* cross section S on temperature. The proportionality of S_{Na,N_2} to T^{-1} in the temperature range covered by the hydrogen–oxygen–nitrogen flames (1760° to 2160°K) points to a value of $q = 2$, within certain error limits, at least in a range of v_r values around the mean value $\bar{v}_r$ in our flames (cf. equation (33) of Part I).

The fact of $\sigma(\bar{v}_r)$ values found by other authors pointing to a decrease of $\sigma(v_r)$ with decreasing v_r for *low* v_r values (see Fig. 9) seems to invalidate our assumption of a constant exponent q in equation (11). However, when we take an average over a Maxwellian velocity distribution of v_r at flame temperature, the contribution of the initial ($v_r \ll \bar{v}_r$) and final ($v_r \gg \bar{v}_r$) parts of the $\sigma(v_r)$ function to the effective (that is, averaged) cross section S is not very important (see Part I). When, for example, $\sigma(v_r)$ is set equal to zero for $v_r < v_r'$

and to b'/v_r^2 for $v_r \geq v_r'$ (b' being a constant of proportionality), we have, as can easily be shown,

$$b' \exp[-\tfrac{1}{2}\mu(v_r')^2/kT] = b$$

where, if we assume equation (11) to be valid, with constant exponent $q = 2$, for any $v_r > 0$, b represents the constant of proportionality that would follow from equation (33)

TABLE 5. REPORTED QUENCHING CROSS SECTION S FOR Na-DOUBLET AT DIFFERENT (MEAN) RELATIVE VELOCITIES $\bar{v}_r$

Quenching species	Experiment	$\bar{v}_r \times 10^{-5}$ (cm sec^{-1})	$S \times 10^{16}$ (cm^2)	References
Ar	Resonance fluorescence (vessel)	1·3	3·0	KONDRATIEV,[34] 1963
		1·8	2·8	KONDRATIEV and SISKIN,[33] 1935
Ar	Resonance fluorescence (flame)	1·9	2·3	This work
Ar	Line-reversal (shock tube)	2·2	$(1{\cdot}0 \times 10^{3})$	TSUCHIYA,[26] 1963
Ar	Excitation by sparks (vessel)	2·8	3·3	KONDRATIEV and SISKIN,[22] 1935
He	Direct determination of lifetime	0·9	0·34	DEMTRÖDER,[25] 1962
H_2	Resonance fluorescence (vessel)	2·5	23·	NORRISH and SMITH,[27] 1945
H_2	Excitation by sparks (vessel)	3·1	11·	WINANS,[21] 1930
H_2	Excitation by sparks (vessel)	3·3	11·	WINANS,[21] 1930
H_2	Resonance fluorescence (flame)	4·6	15·5	This work
H_2	Resonance fluorescence (flame)	4·8	14·	This work
O_2	Resonance fluorescence (flame)	1·75	66·	This work
O_2	Excitation by sparks (vessel)	1·8	52·	KONDRATIEV and SISKIN,[33] 1935
O_2	Resonance fluorescence (flame)	1·80	62·	This work
H_2O	Resonance fluorescence (vessel)	2·0	1·0	This work
CO	Resonance fluorescence (vessel)	0·9	88·	NORRISH and SMITH,[27] 1945
CO	Resonance fluorescence (flame)	1·66	85·	This work
CO	Line-reversal (shock tube)	2·2	43·	TSUCHIYA,[26] 1963
CO	Excitation by sparks	2·5	12·5	KISELBASCH, KONDRATIEV and LEIPUNSKII,[23] 1932
CO_2	Resonance fluorescence (flame)	1·56	113·	This work
CO_2	Resonance fluorescence (flame)	1·61	106·	This work
CO_2	Resonance fluorescence (flame)	1·70	94·	This work
CO_2	Excitation by sparks (vessel)	1·8	53·	WINANS,[21] 1930
N_2	Resonance fluorescence (vessel)	0·9	45·	NORRISH and SMITH,[27] 1945
N_2	Direct determination of lifetime	0·9	42·	DEMTRÖDER,[25] 1962
N_2	Direct determination of lifetime	0·9	37·	HULPKE, PAUL and PAUL[24] 1964
N_2	Resonance fluorescence (vessel)	1·0	90·	VON HAMOS[22] 1932
N_2	Resonance fluorescence (flame)	1·70	44·	This work
N_2	Resonance fluorescence (flame)	1·80	40·	This work
N_2	Resonance fluorescence (flame)	1·90	37·	This work
N_2	Line-reversal (shock tube)	2·15	45·	TSUCHIYA,[26] 1963
N_2	Excitation by sparks (vessel)	2·60	20·	KISELBASCH, KONDRATIEV and LEIPUNSKII,[22] 1932
N_2	Excitation by sparks (vessel)	2·85	32·	KISELBASCH, KONDRATIEV and LEIPUNSKII,[22] 1932
N_2	Excitation by sparks (vessel)	2·85	29·	WINANS,[21] 1930

of Part I in the flame experiments. If, as a trial for v_r', we insert the mean relative velocity, 100 000 cm/sec, corresponding to the actual temperature, 550°K, in the experiments of VON HAMOS and others (see Fig. 10), we find that b' would differ from b by only 30 per cent.

This does show the relatively small influence of the initial part ($v_r < 100\,000$ cm/sec) of the $\sigma(v_r)$ function on the S value at flame temperature.

In addition to the data inserted in Fig. 9, several S values obtained from different experiments on quenching of excited sodium ($3^2P_{1/2,3/2}$) atoms by various other quenching particles are listed in Table 5 and arranged for comparison according to increasing $\bar{v}_r$.

With regard to argon as a quencher, we learn from Table 5 that the $S_{Na,Ar}$ value found by TSUCHIYA[26] in shock tube experiments at $T = 2750$°K deviates by orders of magnitude from the values found by other authors for argon and helium. TSUCHIYA imputes this discrepancy to the impurities present in the inert gas used in the other experiments. Starting from TSUCHIYA's low value for argon, however, we would have to assume an unusually strong temperature dependence of S_{Na,H_2O}—as $S_{Na,H_2O} \propto 1/T^4$—in order to explain the overall quenching effects found in our stoichiometric hydrogen–oxygen–argon flames No. 1, 2, and 3 (see Table 1). Moreover, the reasonable agreement among the $S_{Na,Ar}$ values found by all other authors (see Table 5) makes any explanation based on unwonted impurities improbable. It should be noted that SOBOLEV and coworkers[28] also found a value of $S = 1{\cdot}2 \times 10^{-16}$ cm^2 in their experiments on shock-heated argon for barium ions in the $6P_{1/2,3/2}$ state, which agrees more closely in order of magnitude with our $S_{Na,Ar}$ value than it does with TSUCHIYA's value. Theoretical calculations by NIKITIN and BYKHOVSKI[29] on $S_{Na,Ar}$ for the sodium P state also led to values of the order of 10^{-16} cm^2 when the matrix element of the operator of the spin-orbital interaction between the intermediate states $X^2\Sigma$ and $A^2\Pi$ was assumed to be of the order of 350 cm^{-1}. It should be noted also that the quenching cross section of helium atoms in collision with sodium ($3P$) atoms, found experimentally by DEMTRÖDER,[25] appears to be of the order of 10^{-16} cm^2 (see Table 5). However, recent theoretical calculations and discussions by STAMPER[30] point to an $S_{Na,He}$ value that is less than DEMTRÖDER's experimental value by several orders of magnitude.

Although the value of $S_{Na,Ar}$ is neither experimentally nor theoretically firmly established, we are inclined to believe its value to be of the order of 10^{-16} cm^2, because of the reasonable agreement among all but TSUCHIYA's experimental results (see Table 5).

Comparing the S values found for CO as a quencher of excited sodium atoms (see Table 5), we note a uniform decrease of S value with increasing $\bar{v}_r$ value. The same behaviour is found for N_2 for $\bar{v}_r$ values ranging from 10^5 to $2{\cdot}5 \times 10^5$ cm/sec (see Fig. 10). However, such a decrease disagrees with the prediction of quantum mechanical calculations on collisional energy transfer between electronic and vibrational degrees of freedom, as performed by DICKENS, LINNETT and SOVERS.[31] They instead found a uniform increase of quenching cross section $\sigma(v_r)$ with increasing v_r for all values of v_r. It should be noted, however, that their theoretical prediction of a resonance effect in the quenching of excited mercury atoms, $6^3P_1 \rightarrow 6^3P_0$, by nitrogen molecules agrees qualitatively with our observations on the quenching of excited sodium atoms (see Fig. 7). On the other hand, it appears that the absolute value of S_{Na,N_2} calculated by DICKENS, *et al.*, is less than the experimentally well-established value by many orders of magnitude. In agreement with the experiments of NORRISH and SMITH,[27] our flame experiments yield a relatively large effective quenching cross section for the unsaturated carbon monoxide molecule, compared to those of the other diatomic molecules (H_2, O_2, and N_2) on the basis of an equal resonance defect (see also Fig. 7).

NOTE ADDED IN PROOF

After our manuscript was received by the Editors of this Journal, a short article by JENKINS[36] appeared, reporting quenching cross sections of several flame particles (N_2, O_2, H_2, CO_2, CO, H_2O, Ar and He) in collision with excited Na-atoms. These cross sections were determined in flames at atmospheric pressure and with a temperature of about 1800°K, following the experimental procedure outlined in our earlier paper.[2] It appears that JENKINS' cross section values for N_2, O_2, H_2, CO_2, CO and H_2O (see Table 2) are all systematically less than our values by a factor 2, taking into account the (rather small) accidental errors connected with the experimental procedure. No explanation can as yet be given for the systematic difference between JENKINS' and our results. It may be noted that any error in the instrumental conversion factor that relates our relative reemission signals to absolute p-values seems to be excluded by the mutual consistency between the outcome of our resonance fluorescence measurements and that obtained *independently* from our measurements of the deviation of the line-reversal temperature (see Section 10).

Acknowledgment—The authors would like to thank H. F. Tijhaar for his assistance in the experimental work.

REFERENCES

1. H. P. HOOYMAYERS and C. TH. J. ALKEMADE, *JQSRT* **6**, 501 (1966).
2. A. L. BOERS, C. TH. J. ALKEMADE and J. A. SMIT, *Physica* **22**, 358 (1956).
3. C. TH. J. ALKEMADE, *Proceedings of the Xth Colloquium Spectroscopicum Internationale*, Spartan Books, Washington (1963).
4. H. P. HOOYMAYERS, Thesis, University of Utrecht, to be published.
5. C. TH. J. ALKEMADE and W. J. LAVEN, *Appl. Sci. Res.* **B6**, 337 (1956).
6. W. SNELLMAN, Thesis, University of Utrecht (1965).
7. TJ. HOLLANDER, Thesis, University of Utrecht (1964).
8. R. HERRMANN and C. TH. J. ALKEMADE, *Flammenphotometric*. 2nd edn., Springer (1960), English translation, Interscience (1963).
9. P. J. TH. ZEEGERS, Thesis, University of Utrecht, to be published.
10. A. G. GAYDON and H. G. WOLFHARD, *Flames, their Structure, Radiation and Temperature*, Chapman and Hall, London (1960).
11. J. D. WINEFORDNER and T. J. VICKERS, *Analyt. Chem.* **36**, 161 (1964).
12. E. HINNOV and H. KOHN, *J. Opt. Soc. Am.* **47**, 151 (1957).
13. C. VAN TRIGT, TJ. HOLLANDER and C. TH. J. ALKEMADE, *JQSRT* **5**, 813 (1965).
14. F. W. HOFFMANN and H. KOHN, *J. Opt. Soc. Am.* **51**, 512 (1961).
15. W. BEHMENBURG, H. KOHN and MAILÄNDER, *JQSRT* **4**, 149, 163 and 177 (1964).
16. G. HERZBERG, *Spectra of Diatomic Molecules*, 2nd edn., Van Nostrand, New York (1950).
17. G. HERZBERG, *Infrared and Raman Spectra of Polyatomic Molecules*, Van Nostrand, N.Y. (1954).
18. A. C. G. MITCHELL and M. W. ZEMANSKY, *Resonance, Radiation and Excited Atoms*, 2nd edn., Cambridge Univ. Press, Cambridge (1961).
19. A. G. HEARN, *Proc. Phys. Soc. Lond.* **84**, 11 (1963).
20. A. TERENIN and N. PRILESHAIEVA, *Z. Phys. Chem.* **B13**, 72 (1931).
21. J. G. WINANS, *Z. Phys.* **60**, 631 (1930).
22. L. VON HAMOS, *Z. Phys.* **74**, 379 (1932).
23. B. KISELBASCH, V. KONDRATIEV and A. LEIPUNSKII, *Sov. Phys.* **2**, 201 (1932).
24. E. HULPKE, E. PAUL and W. PAUL, *Z. Phys.* **177**, 257 (1964).
25. W. DEMTRÖDER, *Z. Phys.* **166**, 42 (1962).
26. S. TSUCHIYA, *J. Chem. Soc.* Japan **37**, 6 (1964).
27. R. G. W. NORRISH and W. SMITH, *Proc. R. Soc.* **176A**, 295 (1945).
28. N. N. SOBOLEV, *et al.*, *Proceedings of Fifth International Conference on Ionisation Phenomena in Gases*, North-Holland, Amsterdam (1962).
29. E. E. NIKITIN and V. K. BYKHOVSKI, *Optics and Spectrosc.* **17**, 444 (1964).

30. J. H. STAMPER, *J. Chem. Phys.* **43**, 759 (1965).
31. P. G. DICKENS, J. W. LINNETT and O. SOVERS, *Discuss. Faraday Soc.* **33**, 52 (1962).
32. W. ORTHMANN and P. PRINGSHEIM, *Z. Phys.* **35**, 626 (1926).
33. V. KONDRATJEW and M. SISKIN, *Phys. Z.* **8**, 644 (1935).
34. V. N. KONDRATIEV, *Dokl. Akad. Nauk SSSR* **153**, 1108 (1963).
35. C. W. ALLEN, *Astrophysical Quantities*, University of London, The Athlone Press, London (1955).
36. D. R. JENKINS, *Chem. Commun.* **6**, 171 (1966).

APPENDIX: DEPENDENCE OF FLUORESCENCE INTENSITY ON METAL CONCENTRATION

Under the conditions described in Section 3, we can write for the total energy absorbed by the metal atoms in the flame volume $O\,\mathrm{d}x$ (O is the small constant cross section of the incident light beam, see Fig. 2).

$$O\,\mathrm{d}x\int_0^\infty \mathrm{d}\nu I_\nu \exp(-\varkappa_\nu x)\varkappa_\nu$$

where I_ν is the energy per second at frequency ν of the incident light beam per unit area and per unit frequency interval, and $\varkappa_\nu\,\mathrm{d}x = \beta_\nu N_0\,\mathrm{d}x$ is the fraction of energy absorbed at frequency ν when the exciting light beam travels over a distance $\mathrm{d}x$ in the flame.

The intensity of fluorescence radiation emitted by the irradiated flame volume in a direction perpendicular to the direction of the exciting light beam through a small solid angle ω is equal to (see Fig. 2)

$$\frac{\omega O}{4\pi}\left[\int_0^\infty \mathrm{d}\nu I_\nu \exp(-\varkappa_\nu x)\varkappa_\nu \int_0^\infty \mathrm{d}\nu' p\alpha_{\nu'} \exp(-\varkappa_{\nu'} y)\right]\mathrm{d}x \tag{A1}$$

where p is the fluorescence yield factor and $\alpha_\nu\,\mathrm{d}\nu$ is the probability of a re-emitted photon having a frequency between ν and $\nu+\mathrm{d}\nu$. According to classical radiation theory, we have $\alpha_\nu = (\text{constant})\beta_\nu$. The validity of this relation can also be assumed for our fluorescence experiments, since ORTHMANN and PRINGSHEIM[32] have shown that, even under conditions of lower total gas pressure, the frequency distribution of resonance radiation emitted at right angles to the direction of the exciting beam is independent of the spectral shape of the exciting line. In these experiments, secondary and tertiary resonance radiation could be neglected.

In the low density case, we can replace the exponential function by the first two terms of its series expansion, so that equation (A1) changes to

$$\frac{\omega O}{4\pi} p\left[\int_0^\infty \mathrm{d}\nu \int_0^\infty \mathrm{d}\nu' I_\nu \alpha_{\nu'} \varkappa_\nu (1-\varkappa_\nu x-\varkappa_{\nu'} y)\right]\mathrm{d}x$$

where terms of second and higher order in $\varkappa_\nu$ are neglected. Realizing that y is a function of x and performing the integration over x, we obtain for the total radiant flux of the fluorescent radiation observed,

$$\begin{aligned} E_r &= \frac{\omega p}{4\pi} V N_0 \int_0^\infty \mathrm{d}\nu \int_0^\infty \mathrm{d}\nu' \beta_\nu \alpha_{\nu'} I_\nu - N_0^2 \int_0^\infty \mathrm{d}\nu \int_0^\infty \mathrm{d}\nu' \alpha_\nu I_\nu \left(\beta_\nu^2 VR + \beta_\nu \beta_{\nu'} V \frac{\pi R}{4}\right) \\ &= \frac{\omega}{4\pi} p(\gamma_1 N_0 - \gamma_2 N_0^2) \end{aligned} \tag{A2}$$

in which V represents the volume of the illuminated part of the flame, while γ_1 and γ_2 are positive constants depending only on the exciting lamp and flame conditions, and not on N_0.

In a similar way, we find, after series expansion, for the radiation flux absorbed by the flame,

$$E_a = N_0 V \int_0^\infty \mathrm{d}\nu I_\nu \beta_\nu - RVN_0^2 \int_0^\infty \mathrm{d}\nu I_\nu \beta_\nu^2 = N_0\gamma_3 - N_0^2\gamma_4. \tag{A3}$$

Using $\int_0^\infty \alpha_\nu \,\mathrm{d}\nu = 1$, we find that $\gamma_1 = \gamma_3$. From this it follows by combining equations (A2) and (A3) that

$$\frac{E_r}{E_a} = \frac{\omega p}{4\pi}\left[1 - N_0\left(\frac{\gamma_2 - \gamma_4}{\gamma_1}\right)\right]$$

where terms of the second and higher orders in N_0 are neglected. Applying

$$\gamma_1 = V \int_0^\infty \mathrm{d}\nu \beta_\nu I_\nu$$

and

$$\gamma_2 - \gamma_4 = V\frac{\pi R}{3} \int_0^\infty \mathrm{d}\nu \int_0^\infty \mathrm{d}\nu' I_\nu \alpha_{\nu'} \beta_\nu \beta_{\nu'}$$

we finally obtain

$$\frac{E_r}{E_a} = \frac{\omega p}{4\pi}\left(1 - N_0 \frac{\pi}{4} R \int_0^\infty \mathrm{d}\nu' \alpha_{\nu'} \beta_{\nu'}\right).$$